Book of Tutorials and Abstracts

European Microbeam Analysis Society

EMAS 2026

15th

REGIONAL WORKSHOP

TOPICAL CONFERENCE ON ELECTRON BACKSCATTER DIFFRACTION (EBSD)

14 to 17 June 2026
at the
CentraleSupélec, Gif-sur-Yvette, France

Organised in collaboration with:
ICMMO, ENS Paris-Saclay,
Université Paris-Saclay

EMAS
European Microbeam Analysis Society eV
www.microbeamanalysis.eu/

This volume is published by:
European Microbeam Analysis Society eV (EMAS)
EMAS Secretariat
c/o Eidgenössische Technische Hochschule, Department of Earth and Planetary Sciences
Clausiusstrasse 25
8092 Zürich
Switzerland

ISBN 978 90 8227 6992
NUR code: 971 – Materials Science

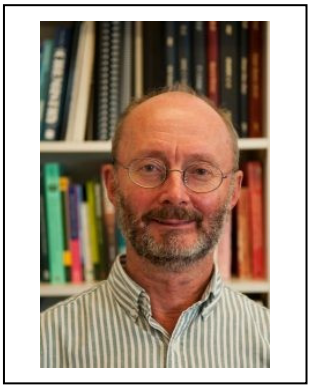

EBSD IN GEOSCIENCES: EXAMPLES OF THREE DEVELOPMENTS IN THREE DECADES

John Wheeler

University of Liverpool, Department of Earth, Ocean and Ecological Sciences
Jane Herdman Building, 4 Brownlow Street, Liverpool L69 3GP, United Kingdom
e-mail: johnwh@liverpool.ac.uk

John Wheeler is the George Herdman Professor of Geology at the University of Liverpool and has a long-standing interest in EBSD. He has a background in researching microstructural and microchemical evolution of rocks and was stimulated by the potential of EBSD for this when the Liverpool laboratory was set up in the 1990s. This was one of the first places to popularise EBSD in geoscience and he contributed via new ideas, methods and specific studies. EBSD is now a well-established tool in geoscience and researchers he has assisted now run EBSD laboratories and research projects around the world. His main activity remains development of quantitative analysis methods and implementing them in software, notably a method to analyse intracrystalline distortion. His work extends to ice and metals and is of general applicability to crystalline materials. Realising this, Oxford Instruments have, since 2021, included one of his techniques in their software releases. His two most recent EBSD papers are on olivine (the most common mineral in the upper 400 km of the Earth) and, as co-author, on GaN (a widely used semiconductor) indicating the breadth of his interests.

1. INTRODUCTION

Geoscientists have an interest in microstructures since they tell us about the histories of rocks and the processes that formed them, primarily those related to deformation. For more than a century we have used optical observations in transmitted and reflected light, and these are enough to reveal grain shapes, sizes and intracrystalline distortion (e.g., quartz with "undulose extinction") which in part relate to deformation. Optical transmitted light observations using a universal stage allow crystallographic preferred orientations (CPOs) to be constrained though not fully determined (e.g., <c> axis CPOs in quartz). In recent decades X-ray goniometry and transmission electron microscopy (TEM) have allowed investigations on sample or micrometre scale. X-ray goniometry gives an overall picture but no information as to where particular orientations are present in a microstructure. TEM is at such high magnification that one must always question how representative the observations are. In the 1980s, geoscientists realised that electron channelling could provide useful microstructural information at intermediate scales [1] but this was soon superseded by EBSD as this is easier to use. EBSD was an established technique in metallurgy years before geoscientists realised how useful it was, but in the 1990s it began to be adopted enthusiastically in that discipline [2]. It provides information on the same scale as optical observations but with added dimensions and can then go to much finer scales and help bridge the scale gap down to TEM if needed. Table 1 is a simple indicator of how EBSD in geoscience has taken off, illustrated via counting mentions of quartz (trigonal) or olivine (orthorhombic), two common and interesting minerals.

Table 1. Number of papers from Web of Science search for "(ebsd or "electron backscatter") and (quartz or olivine)" in any field.

Decade	**Number of papers**
1981-1990	0
1991-2000	16
2001-2010	147
2011-2020	582

In this contribution I will give examples of three developments over three decades in the way we use EBSD data, with the aim of provoking general discussion. I will include small old datasets and large recent ones and reflect on the extent to which the extra data add to our understanding. I focus on my own experience, which is mainly in interpreting what we might call "standard" EBSD data, the three numbers that define crystal orientation at a point. I will not address the many stimulating developments in analysing Kikuchi patterns for strain, chirality, pseudosymmetry and so forth although these will be as relevant for geoscience as for other disciplines. The three analysis approaches are given in order of development, which reflects increasing complexity or detail. For broader but less up to date views of EBSD in geoscience see [3] and [2].

a) Crystallographic preferred orientations: These often give information on deformation, as in other crystalline materials. They always tell us something about how the rock formed. They do not make full use of the spatial distribution of orientations, though one can of course define subareas and look at CPO differences.
b) Misorientation: Calculated differences in orientation from one measured point to another. Knowing the positions of measurement points allows us to examine misorientation across particular structures and along transects.
c) Intracrystalline orientation gradients: A refinement in misorientation analysis in which we combine spatial and orientation data to make numerical estimates of orientation gradients in perhaps smoothly distorted crystals. These can then be linked to the presence, type and density of geometrically necessary dislocations (GNDs).

2. CRYSTALLOGRAPHIC PREFERRED ORIENTATIONS

Since we have the full orientation at every EBSD point we can plot the CPO of any axis. Such figures often show non-random patterns indicating anisotropy, called "fabric" in geoscience and "texture" in metallurgy. In deformed rocks, where a large region is sampled composed of many original grains, they can tell us about the type of strain and the slip systems active which in turn relate to temperature and other imposed parameters.

2.1. Quartz - naturally deformed

Fig. 1 shows a deformed quartz vein [4] and Fig. 2 shows pole figures from a low strain area, where large elongate grains were diagnosed as "relict" and small, likely new, grains as "matrix". In this case the area is too small to get an overall picture of CPO, but <c> axes in Fig. 2a) show there are three main relict grains. This is early EBSD work, before mapping was routine, and grains were identified by tracing boundaries from forescatter (orientation contrast) images.

Fig. 2b) shows the <a> axes (which cannot be measured optically) from those grains, showing a wide range in orientations. The clustering of <c> versus the spread in <a> indicates likely non-basal slip operating in these grains; it looks like orientations vary within grains by rotations around <c>. Such deductions overlap with those of misorientation analysis considered later.

2.2. Olivine - experimentally deformed

Fig. 3 shows experimentally deformed olivine [5] and epitomises the advances made in EBSD in 30 years – Fig. 2 displays 738 points whilst this map has 7,968,000 points, mostly indexed. We now have a grid of measurement points, and each point is colour coded according to orientation on an inverse pole figure. We have no further need to use forescatter images as maps.

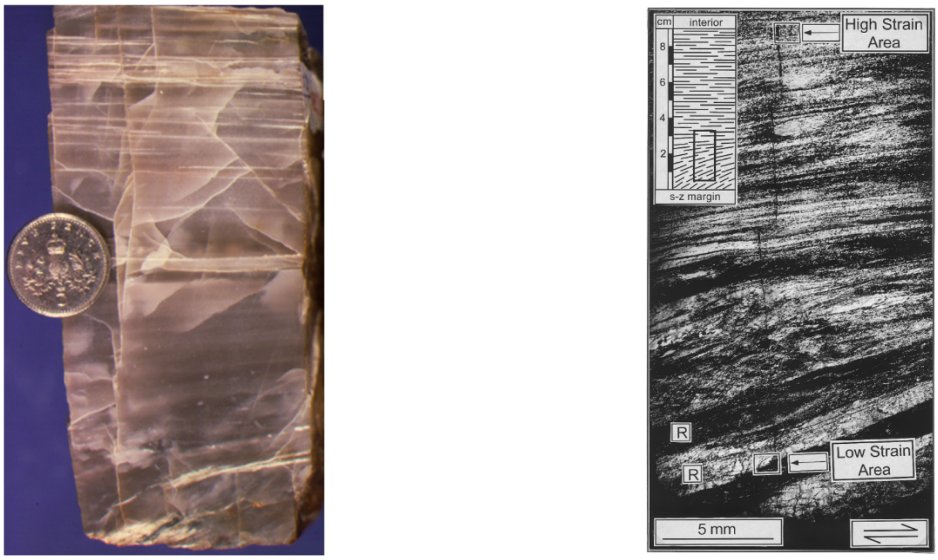

Figure 1. Left: Photo of shear zone in quartz vein, with low strain at bottom. Right: Optical image of strain gradient taken under cross-polarised light.

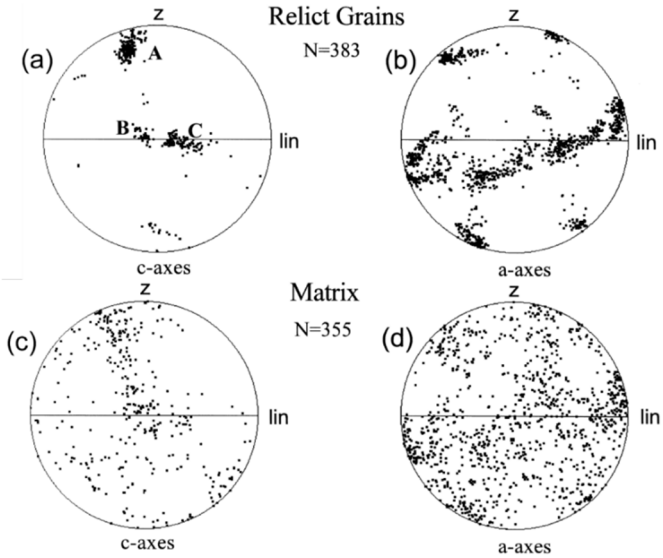

Figure 2. Pole figures from part of the shear zone of Fig, 1; “lin”, meaning lineation, is the shear direction.

Olivine has dominant dislocation slip systems with Burgers vectors parallel to a = [100] or c = [001]. Pole figures (Fig. 4) show that <c> is on average strongly aligned with the maximum extension, suggesting that was the Burgers vector of the main slip system. As will be shown later, this is an oversimplification. The pole figures take no account of the spatial distributions of orientations, yet these clearly show patterns: for example, the smooth colour variation from orange to green in one top right grain indicates organised internal strain gradients.

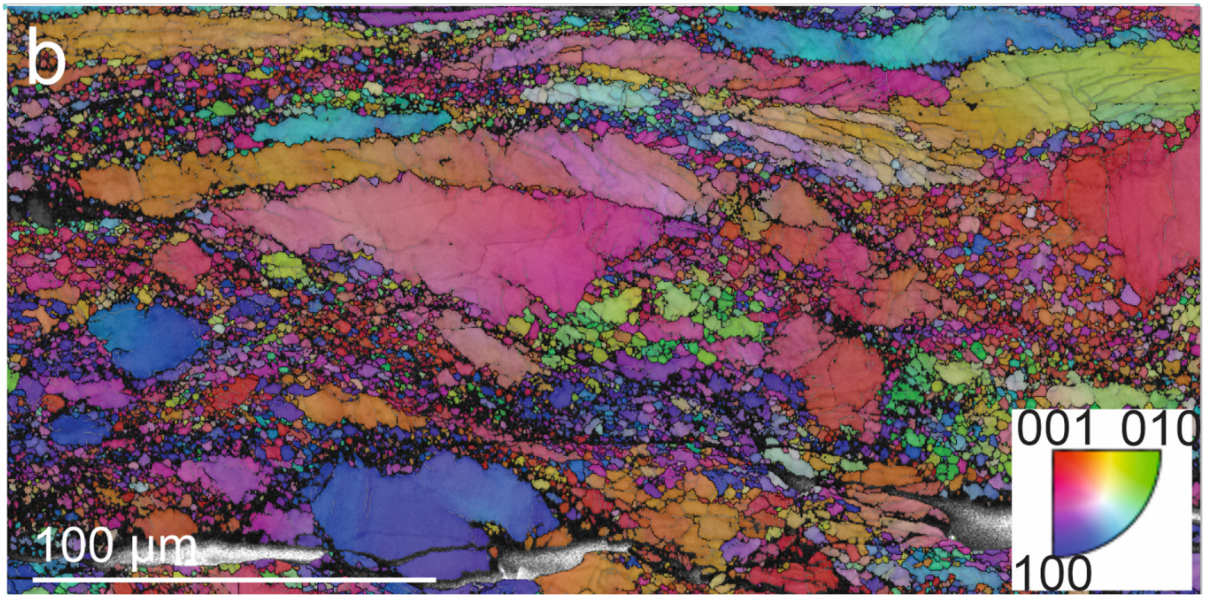

Figure 3. EBSD map of experimentally deformed olivine colour coded by the direction of maximum extension in crystal coordinates (Inverse Pole Figure key in bottom right).

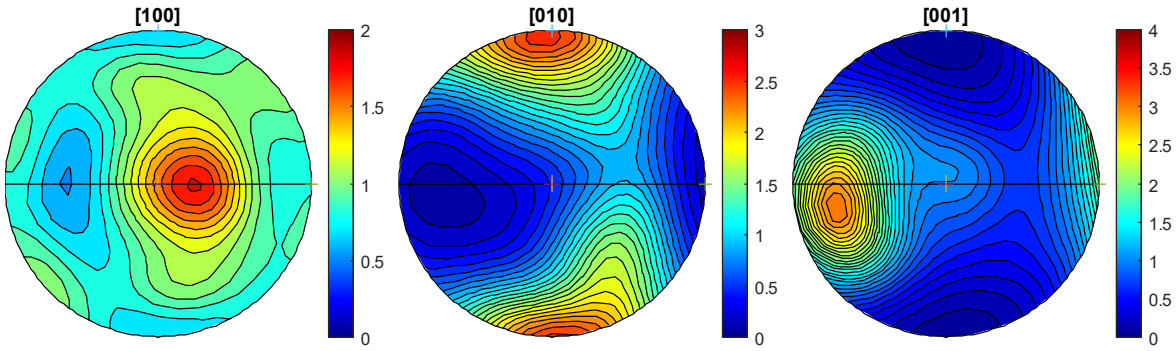

Figure 4. Contoured olivine pole figures for the map in Fig. 3.

3. MISORIENTATION

Misorientation is defined as the difference between two orientations (Fig. 5). If P and Q are rotation matrices denoting orientations and M is the misorientation then $Q = MP$ so $M = QP^{-1}$. Mathematical variations on this relate to whether M is expressed in crystal or sample coordinates [6]. In either case M, like all rotation matrices, can be expressed as a rotation axis (unit vector with 2 independent components) and a rotation angle. When crystals have symmetry, more than one misorientation can be defined. In Fig. 5 we see the same cube can be rotated in two different ways to a final orientation. In the figure the corners are labelled with stars and the outcomes are recognisably distinct but in reality, there are no such labels and there may be many axis/angle pairs to represent misorientation. By convention we select the minimum misorientation angle (then sometimes called “disorientation”) and its associated axis.

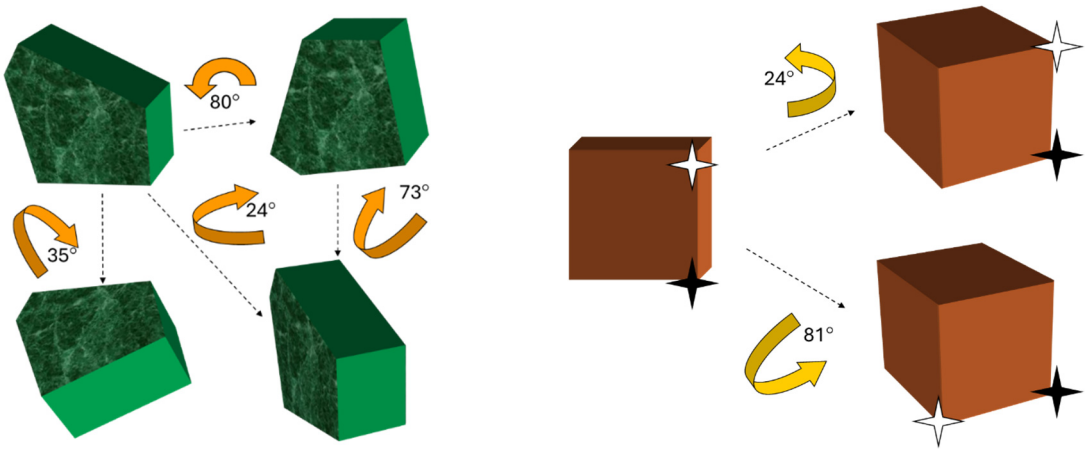

Figure 5. Left: examples of misorientations of irregular objects. Right: Crystal symmetry gives rise to multiple possible misorientations.

Misorientation axes and/or angles provide useful information in geoscience. So far as I am aware, the first geoscience application of misorientation analysis was on quartz [7], based on an EBSD map but years elapsed before such approaches became routine; the same map was re-used six years later [8].

3.1. Quartz - experimentally deformed

First, I give an example of the statistics of angles using an experimentally deformed quartz sample [9]. First select pairs of points from random positions in the microstructure, calculate the misorientations and plot the angles as in Fig. 6a [6]. The red graph indicates the expected probability distribution for random pairs selected from a randomly oriented distribution. The blue histogram differs from it only because the deformed quartz has a CPO and so there is more chance of finding a lower misorientation angle between two points than if the orientations were random. There is no additional geological significance to the difference. In Fig 6b, we harness the knowledge of relative positions and undertake the same exercise but for neighbouring measurement points. There are significant differences between the random pair and neighbour pair histograms which are of geological significance. The Kolmogorov-Smirnov test is a rigorous statistical method for determining whether differences are "significant" [6] but there seems little appetite for its use and differences are often fairly obvious. Wheeler *et al.* [6] suggested a general framework for understanding such differences: they mean:
1. Neighbouring grains have undergone a physical interaction, and/or
2. They have been inherited from a common parent.

The development of sub-grain walls during deformation is an example of inheritance. In Fig 6, we see there are relatively large counts of low misorientations, a pattern in accord with recovery during deformation forming sub-grain walls within original single grains. There is also a spike at 60° indicating deformation induced Dauphine twins.

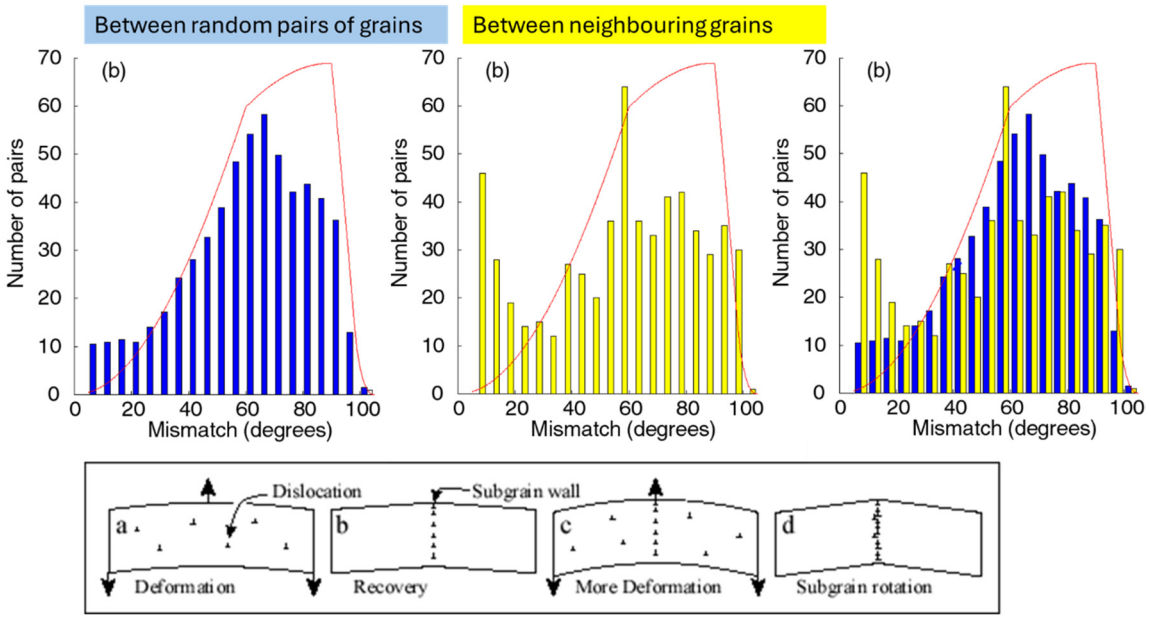

Figure 6. Histograms of misorientation angles from deformed quartz: a) Random pairs, b) Neighbour pairs, c) Both. Red graph indicates expected probability distribution for random pairs selected from a randomly oriented distribution (i.e., no CPO).

3.2. Quartz - naturally deformed

We can examine the spatial distribution of boundaries with different misorientations. Fig. 7 is from the same study as Fig. 1 etc. and shows all boundaries above 4° and 10° in the low strain zone. We see hints of a gradual decrease in abundance of boundaries over a wide angular range, with original grains still recognisable.

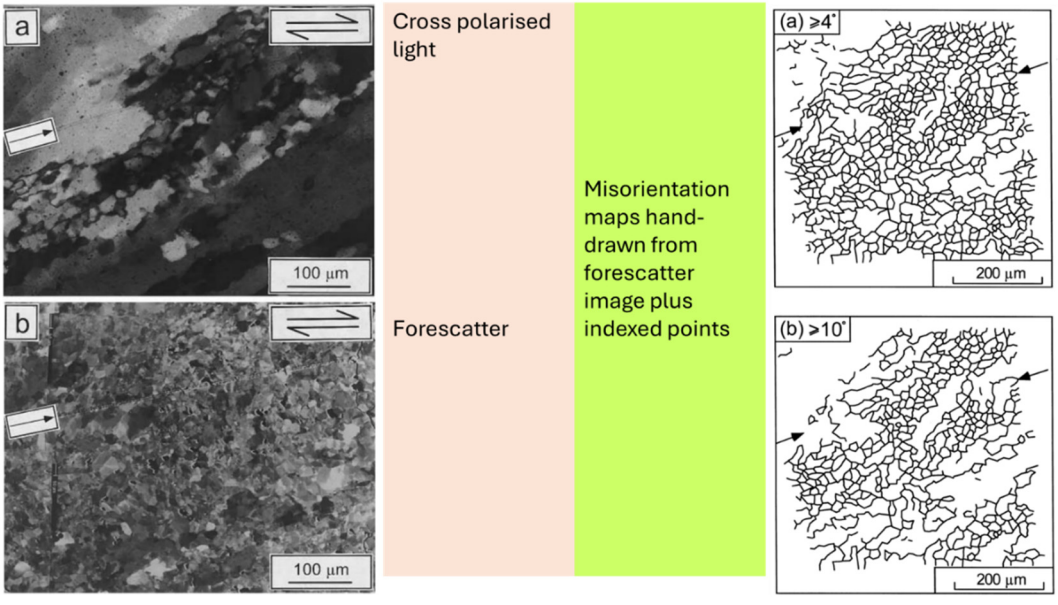

Figure 7. Images and hand-drawn boundaries from the low strain part of the quartz shear zone.

This is reflected in the histogram in Fig. 8a but in contrast the matrix histogram in Fig. 8b shows a sharp decrease in abundance. An interpretation is that in the relict grains we are seeing mainly recovery and sub-grain rotation recrystallisation whilst in the matrix we have additional processes including grain boundary sliding. The latter would involve rotations across many boundaries, obliterating their original organised low angle natures. Regardless of whether this is correct, the misorientation analysis gives insights into the evolution.

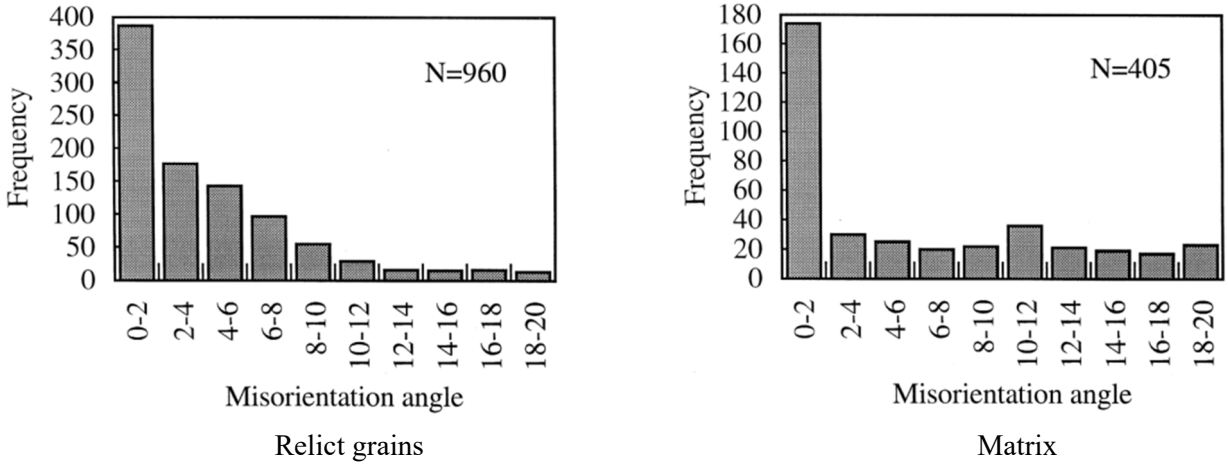

Figure 8. Frequencies of boundaries in range up to 20° in different microstructural settings in the quartz shear zone.

3.3. Albite - naturally deformed

Figure 9 offers a different story from a rock with albite (triclinic) layers deformed to high strain [10]. Two sub-areas are identified based on contrasting grain size. Figs. 10b and 10c show that, unlike in the previous examples, the random pair and neighbour pair histograms are similar to each other in subareas E1 and E2 (considered separately). It seems there is no evidence for interaction or inheritance. In fact, Jiang *et al.* [10] argue on other grounds that E1 and E2 were derived from two separate large plagioclase grains. Chemical reaction involved nucleating small new albites in the original plagioclases and the aggregate then deformed by diffusion creep. There was no intracrystalline plasticity hence no fingerprint of sub-grain walls etc., and since grain boundary sliding is an intrinsic part of diffusion creep, this would have destroyed any original orientation relationships if there were any. Note that Fig. 10a does, in contrast, indicate big differences between the histograms but this is because many random pairs straddle the two domains and have high angle misorientations. Care is required to interpret such information.

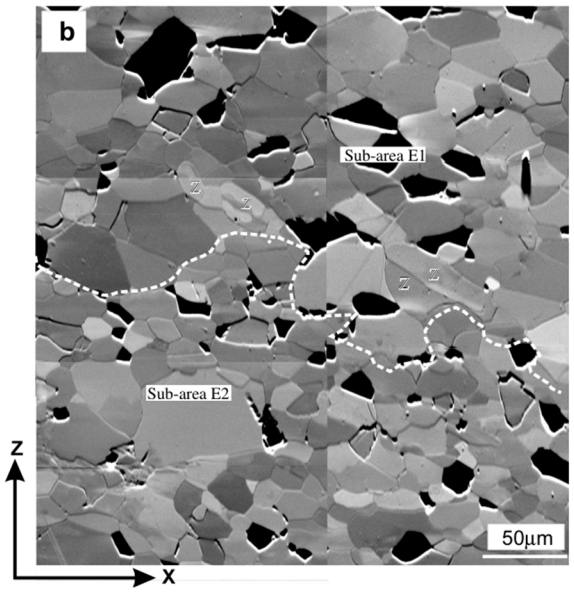

Figure 9. Forescatter image of deformed polycrystalline albite, divided into two sub-areas based on contrasting grain sizes.

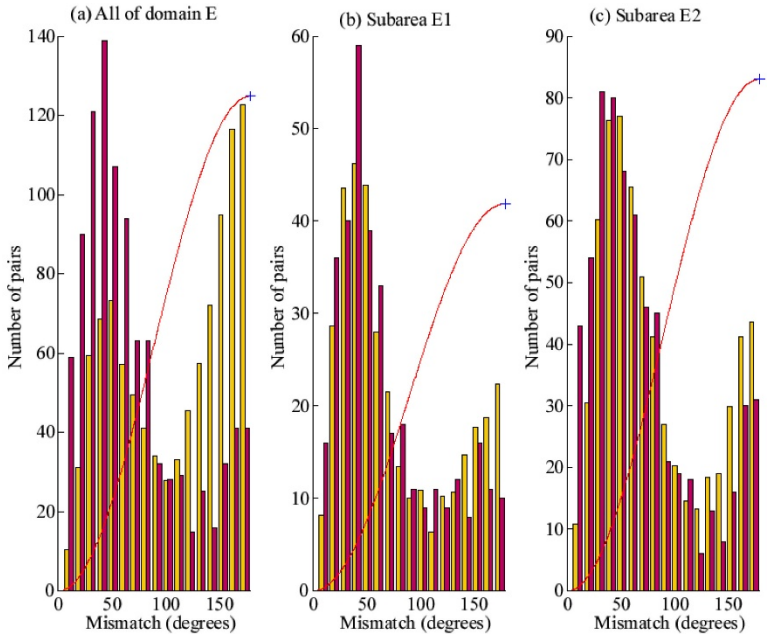

Figure 10. Random-pair (yellow) and neighbour-pair (orange) histograms for albite as in Fig. 9.

3.4. Quartz - naturally deformed (second example)

Misorientation axes must be interpreted with caution. If one assumes that low angle boundaries (LABs, say < 10°) are made of organised, geometrically necessary dislocations then misorientation axes give information on slip systems. Common assumptions are that the LABs in question are tilt walls and made of a single type of edge dislocation in which case the

misorientation axis is parallel to the dislocation line and perpendicular to the Burgers vector. Fig. 11 shows misorientation axes for two quartz samples [11] naturally deformed at different temperatures [12]. In the 2 - 10° range, we see that I2 is compatible with basal slip (basal slip plane (c) and Burgers vector parallel to <a>) and I9 is compatible with a prismatic slip plane such as (a). Such deductions are in accord with our understanding of temperature effects on quartz slip systems [13]. Note that is not straightforward to test the "standard" assumptions but at least they should be stated. There are prominent maxima parallel to the <c> axis for 30 - 60° in both samples. This is the correct misorientation axis for Dauphiné twinning, but the low angles are a long way off the expected 60° so some other process (not yet characterised) must have modified them. Misorientation analysis may not be in accord with slip systems deduced from CPOs – for example in a study of deformed quartzites from Scotland the overall CPO would be interpreted as being influenced by (c)<a> slip but misorientation axes are oriented parallel to <c> [14]. To explain the discrepancy that work postulated the LABs had a twist component. The next section describes additional analysis that might help resolve such issues.

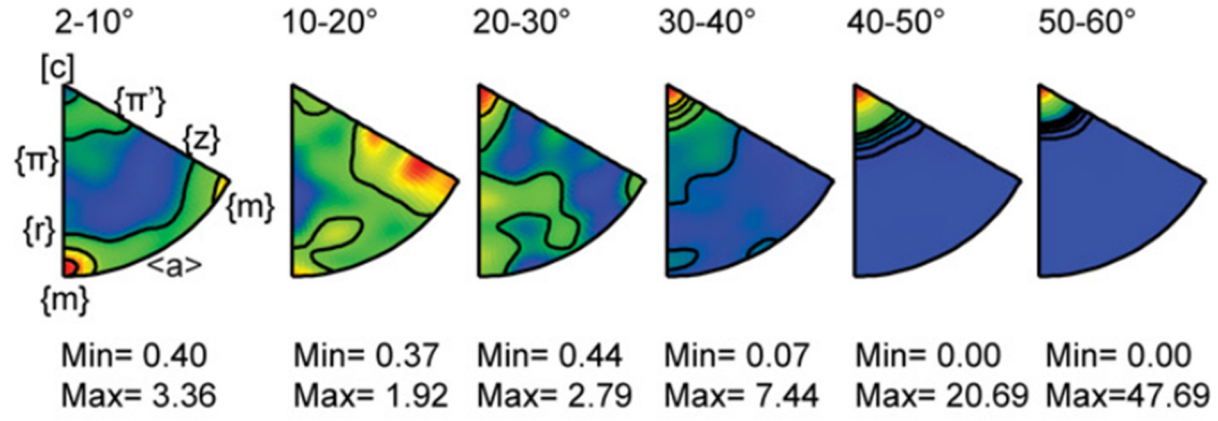

Sample I2 deformed at 300 - 450 °C

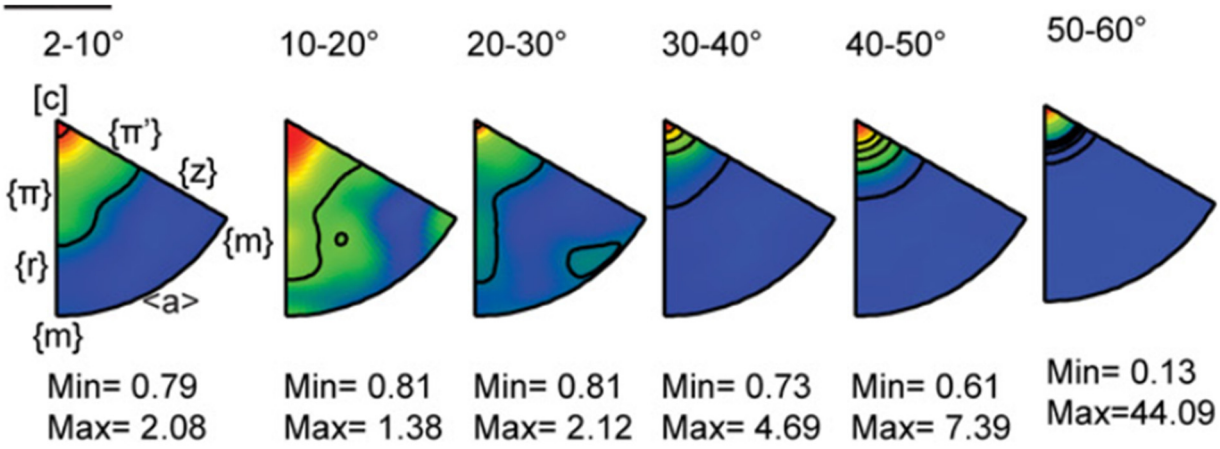

Sample I9 deformed at 520 - 630 °C

Figure 11. Misorientation axes for various ranges of misorientation angle for two naturally deformed quartz samples.

4. INTRACRYSTALLINE ORIENTATION GRADIENTS

Misorientation is just the difference between two orientation values, defined using matrix algebra. The two measurements may be far apart, or either side of a boundary in which case we can get information on GNDs in that boundary. But GNDs can also give rise to smooth lattice curvature. Turning this round, boundaries can be considered as mathematical limits of strongly curved lattices [15] so there is much overlap in the ideas and the maths. In principle then we can use lattice curvature to deduce information about the density and types of GNDs. Lattice curvature is a second rank tensor with 9 components defined (leaving out rigorous detail) by

$$\boldsymbol{\kappa} = \boldsymbol{\nabla}(\mathrm{m}\mathbf{n}) \tag{1}$$

where $\boldsymbol{\nabla}$ is the gradient operator, m is misorientation angle relative to the point at which curvature is to be calculated, and **n** is the misorientation axis vector. In more detail the maths to go from here to GND density is subtle, and care must be taken with coordinate systems (crystal versus sample) and even with potentially ambiguous notation [16, 17]. Here let me outline the key things to be aware of without going into all the maths. First, curvature.

- Usually, we have only two dimensions of EBSD data so we cannot calculate gradients in the z direction and can get only 6 of the 9 κ components.
- Gradients must be estimated from spaced grid points and since orientation differences are small, misorientation and hence curvature errors will be relatively large even if orientation errors are relatively small [18]. Any curvature calculations will benefit from more accurate orientation measurements such as from high angular resolution EBSD [19] but the way EBSD data are used in subsequent calculations is unchanged.
- Step size, and the number of measurement points used in calculating curvature, have important effects on such calculations.

Secondly, now we have some components of curvature what do we do?

- In this paper I do not address getting elastic strains from Kikuchi patterns so we will assume they are zero: an assumption which seems to be useful in practice.
- In that case the curvature is due to GNDs. It is better to refer to such crystals as “distorted” (a non-genetic term) rather than “deformed” because the curvature might be due to for example growth defects.
- Nye [20] showed how curvature has a direct link to dislocation density (line length per unit volume in 3D) via a second rank tensor **α** (which now carries his name), also a function of orientation gradients. This links to dislocation density as follows:

$$\alpha_{i\gamma} = \sum_N \rho^{(N)} b_i^{(N)} l_\gamma^{(N)} \tag{2}$$

where ρ, **b** and **l** are the density, Burgers vector and unit line vector for each type (labelled N) of dislocation. There are two options how we use this expression:

1. We might have more slip systems than the 6 available curvature components. In that case postulate that the total dislocation line energy is minimised for all possible choices of Burgers vector and slip plane, to give a unique answer [21, 22]. This involves specifying dislocation line energies.
2. We might extract some information from the curvature without making such assumptions [16, 23].

For reasons of space (and bias!) I will focus on the second option. The two approaches are compatible, but the energy minimisation methods involve assumptions about slip systems and line energies which, given the plethora of minerals we deal with in geoscience, might be hard to justify. In comparison few assumptions are needed in the second option. This delivers a vector, the weighted Burgers vector (WBV), at each point which is a composite of all the Burgers vectors in the vicinity multiplied by weighted versions of the associated line densities (Fig. 12):

$$W_i = \alpha_{i3} = \sum_N \rho^{(N)} b_i^{(N)} l_3^{(N)} = \sum_N \left[\rho^{(N)} l_3^{(N)}\right] b_i^{(N)} \qquad (3)$$

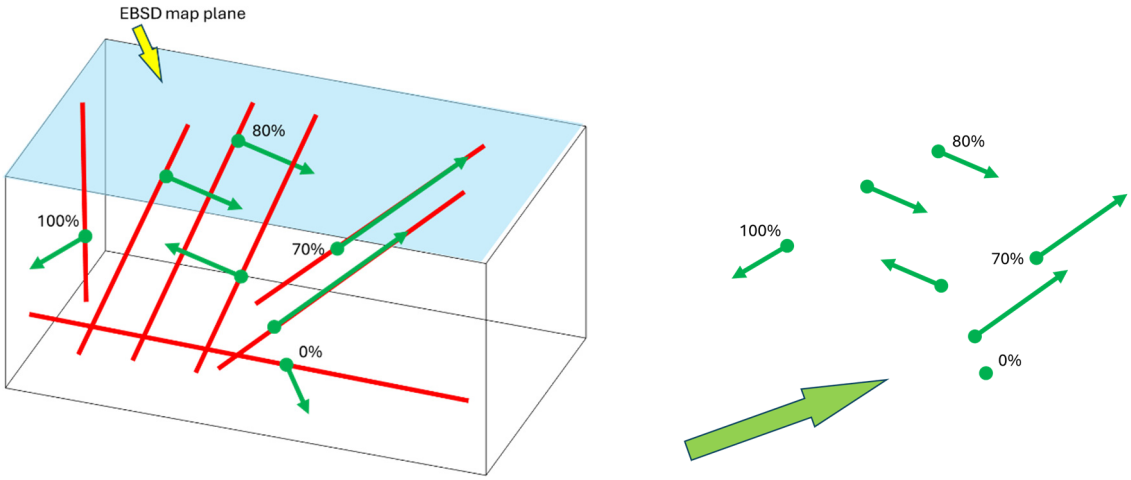

Figure 12. Left: Some dislocation lines (red) and their Burgers vectors (green). Right: Those Burgers vectors are weighted by the sin of the angle that each line makes with the map; the weighting is given as a % and the length of the vector is shortened accordingly. The shortened vectors are summed to give the WBV (thick arrow).

The WBV is in units of (length)$^{-1}$ and its magnitude can be used as a simple proxy for overall GND density, duly noting that the units are different. Magnitude maps highlight areas of high dislocation density. In geoscience WBV direction has been used more than magnitude since it can help identify Burgers vectors. Like any crystallographic vector it can be plotted on pole figures and inverse pole figures and IPF maps can be made. The latter give strong hints of the Burgers vectors of slip systems in operation and may modify understanding of mineral deformation considerably: I give two examples.

4.1. Ice - experimentally deformed

Ice (hexagonal) was long thought to deform plastically by basal slip, with Burgers vectors lying in the basal plane. WBV analysis of experimentally deformed ice revealed vectors at a high angle to the basal plane [24]. Figure 13 shows a box shaped sub-grain with walls colour coded in terms of the (WBV component parallel to <c>)/(WBV magnitude). This is the sin of the angle the WBV makes to the basal plane and clearly that runs up to near 90° in the right-hand wall. Because the WBV is a sum, it cannot be used to uniquely identify the Burgers vectors involved. For example, they could be parallel to <c> or be two symmetric variants of <c + a> combined, but there must be at least one slip system with some sort of non-basal Burgers vector. This approach provides a foundation for more detailed analysis.

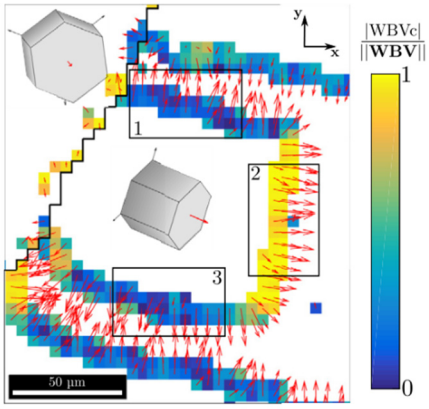

Figure 13. WBV analysis on experimentally deformed ice.

4.2. Olivine - experimentally deformed

A second example concerns olivine. It is commonly asserted that olivine has various slip systems with <a> and <c> Burgers vectors; <b> has been reported but considered so rare as to be unimportant. Consider again the experimentally deformed olivine of Fig. 3. Attention was drawn to the smooth colour variations in the IPF map, indicating intracrystalline distortion. In more detail the distortion is due in part to arrays of sub-grain walls too small to see in that figure. Figure 14 shows a WBV IPF map of a sub-area. There is a distinct green line (inset) suggesting this a sub-grain wall with a <b> Burgers vector. With some difficulty TEM was used to find a <b> dislocation, involving lifting out a wafer from a location identified using the WBV map.

Because the WBV calculation was over the whole map, we could estimate the abundance of <b> dislocations at 17 %. This shows that the common assumption of unimportant <b> is not the case in this sample, and we speculate it will be found to be widespread if the WBV technique is applied more widely. This study also flags a potential issue with the energy minimisation

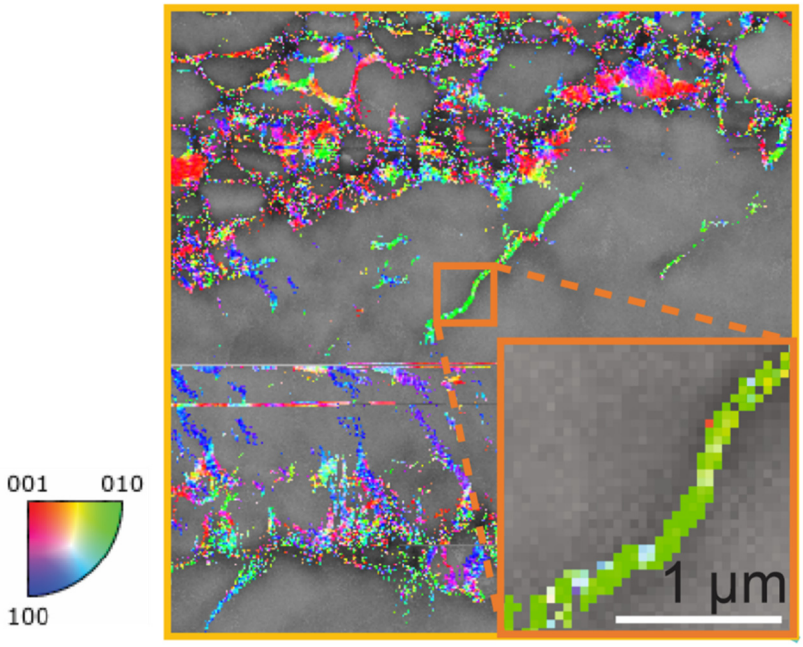

Figure 14. IPF map of WBV from a subarea in top right of Fig. 3. A minimum WBV magnitude is specified otherwise noisy speckled maps result (longer WBVs have smaller angular errors). The horizontal multicoloured lines indicate indexing problems along a few scan lines and should be ignored.

methods mentioned above. In some olivine studies, calculations were "forced" to avoid predicting <b> dislocations: for example, slip systems with [010] Burgers vectors were regarded as "fictitious" and "were assigned Burgers vectors with lengths multiple orders of magnitude larger than the other dislocation types", thus making their energy so high that negligible densities resulted [22]. Perhaps some interesting microstructural features were missed as a consequence.

5. *DISCUSSION*

CPOs: it could be argued that CPOs from EBSD do not provide any more information than CPOs from texture goniometry or other bulk diffraction methods. However, in recent years EBSD data have become fast to obtain and offer the additional advantage of spatially resolved measurements.

Misorientation analysis: this exploits the spatially resolved aspect and can be used to test a variety of hypotheses. In this contribution I focus on deformation related microstructures, but such analysis can be used to understand other processes such as interface energy driven grain rotation [25]. In geoscience and metallurgy, Taylor-Bishop-Hill models and their more sophisticated descendants have long been used to explain CPOs in terms of slip system activity. Misorientation analysis may offer a different picture (e.g., Halfpenny *et al.* [14] mentioned above) and there is work to be done to understand the "efficiency" of slip systems in terms of producing CPO versus their "preservation potential" in terms of GNDs being trapped.

Intracrystalline distortion: analysing this comprises a “deeper dive” into microstructure. As for misorientation analysis, it can be used to understand processes other than deformation – for example topotactic growth of new albite, with associated growth defects, from old plagioclase [26]. It can modify simple views of deformation – for example Fig. 4 could be interpreted as having formed dominantly by slip parallel to <c>, but WBV analysis suggests that GNDs with Burgers vectors parallel to <a> , <b> and <c> are present in ratios roughly 2:1:2, a quite different picture.

All the calculations discussed here are now fast in most academic and commercial software and there is much scope to use them together to improve our understanding of rock evolution.

6. REFERENCES

[1] Lloyd G E, Ferguson C C and Law R D 1987 *Tectonophysics* **135** 243-249

[2] Prior D J, *et al.* 1999 *Amer. Mineralogist* **84** 1741-1759

[3] Prior D J, Mariani E and Wheeler J 2009 *EBSD in the Earth Sciences: Applications, common practice and challenges*. in: Electron backscatter diffraction in materials science. (Schwartz A J, Kumar M, Adams B L and Field D P; Eds.) [New York, NY:Springer] 345-357.

[4] Trimby P W, Prior D J and Wheeler J 1998 *J. Struct. Geol.* **20** 917-935

[5] Wheeler J, *et al.* 2025 *Geophys. Res. Lett.* **52** e2025GL117138

[6] Wheeler J, Prior D J, Jiang Z, Spiess R and Trimby P J 2001 *Contrib. Mineral. Petrol.* **141** 109-124

[7] Kunze K, Adams B L and Wenk H R 1994 Local microstructural investigations in recrystallized quartzite using orientation imaging microscopy. in: Proc. Int. Conf. Textures of Materials (ICOTOM-10) (Bunge H J; Ed.) (Clausthal, Germany; September 1993) *Mater. Sci. Forum* **157-162**. 1243-1250

[8] Heidelbach F, Kunze K and Wenk H R 2000 *J. Struct. Geol.* **22** 91-104

[9] Hirth G and Tullis J 1992 *J. Struct. Geol.* **14** 145-159

[10] Jiang Z, Prior D J and Wheeler J 2000 *J. Struct. Geol.* **22** 1663-1674

[11] Halfpenny A, Prior D J and Wheeler J 2012 *J. Struct. Geol.* **36** 2-15

[12] Stipp M, Stunitz H, Heilbronner R and Schmid S M 2002 *J. Struct. Geol.* **24** 1861-1884

[13] Lister G S, Paterson M S and Hobbs B E *Tectonophysics* **45** 107-158

[14] Halfpenny A, Prior D J and Wheeler J 2006 *Tectonophysics* **427** 3-14

[15] Sutton A P and Balluffi R W 1995 *Interfaces in crystalline materials*. Monographs on the physics and chemistry of materials. [Oxford, UK: Clarendon Press] 819.

[16] Wheeler J, Mariani E, Piazolo S, Prior D J, Trimby P and Drury M R 2009 *J. Microscopy* **233** 482-494

[17] Das S, Hofmann F and Tarleton E 2018 *Int. J. Plasticity* **109** 18-42

[18] Prior D J 1999 *J. Microscopy* **195** 217-225

[19] Wilkinson A J, Meaden G and Dingley D J 2006 *Mater. Sci. Technol.* **22** 1271-1278
[20] Nye J F 1953 *Acta Metallurgica* **1** 153-162
[21] Pantleon W 2008 *Scripta Materialia* **58** 994-997
[22] Wallis D, Hansen L N, Britton T B and Wilkinson A J 2016 *Ultramicroscopy* **168** 34-45
[23] Wheeler J, Piazolo S, Prior D J, Trimby P W and Tielke J AQ 2024 *J. Struct. Geol.* **179** 105040
[24] Chauve T, *et al.* 2017 *Earth Planet. Sci. Lett.* **473** 247-255
[25] Spiess R, Peruzzo L, Prior D J and Wheeler J 2001 *J. Metamorphic Geol.* **19** 269-290
[26] Gardner J, Wheeler J and Mariani E 2021 *Lithos* 396-397 106241